Journal of Magnetic Resonance 201 (2009) 100–110

Contents lists available at ScienceDirect

Journal of Magnetic Resonance

journal homepage: www.elsevier.com/locate/jmr

Thin-film solid-state proton NMR measurements using a synthetic mica substrate: Polymer blends ☆

David L. VanderHart [a], Vivek M. Prabhu [a,*], Kristopher A. Lavery [a,1], Cindi L. Dennis [b], Ashwin B. Rao [a,2], Eric K. Lin [a]

[a] Polymers Division, National Institute of Standards and Technology (NIST), Gaithersburg, MD 20889, USA
[b] Metallurgy Division, National Institute of Standards and Technology (NIST), Gaithersburg, MD 20889, USA

ARTICLE INFO

Article history:
Received 12 April 2009
Revised 9 August 2009
Available online 25 August 2009

Keywords:
Magnetic susceptibility
Mica
NMR
Proton
Resolution
Sensitivity
Solids
Spinning sidebands
Thin film
Polymer blends

ABSTRACT

Solid-state proton nuclear magnetic resonance (NMR) measurements are performed successfully on polymer blend thin films through the use of synthetic mica as a substrate. When used as a substrate, synthetic fluorophlogopite mica with its proton-free, diamagnetic character, allows for adequate measurement sensitivity while minimally perturbing the proton thin-film spectra, especially relative to more commonly available natural micas. Specifically, we use multiple-pulse techniques in the presence of magic-angle spinning to measure the degree of mixing in two different polymer blend thin films, polystyrene/poly(xylylene ether) and poly(1-methyladamantyl methacrylate) (PMAdMA)/triphenylsulfonium perfluorobutanesulfonate (TPS-PFBS), spin-coated onto mica substrates. Our earlier studies had focused on bulk systems where NMR signals are stronger, but may not be representative of thin films of the same systems that are relevant to many applications such as photoresist formulations in the electronics industry. The superiority of synthetic over natural paramagnetic mica is demonstrated by the maintenance of resolution and spinning sideband intensities (relative to bulk samples) for the synthetic mica samples. In contrast, degraded resolution and large spinning sidebands are shown to typify spectra of the natural mica samples. This approach can be applied to many other proton measurements of solid thin films, thereby greatly extending the types of systems to be investigated. Magnetic susceptibility measurements are also reported for all micas used.

Published by Elsevier Inc.

1. Introduction

Solid-state nuclear magnetic resonance (NMR) is a powerful method [1] for measuring the composition, conformation and dynamics, and intimacy of mixing of solid materials. However, the increasingly sophisticated analysis methods that have advanced NMR measurements have not been applicable to the characterization of solid supported thin films. There are enormous opportunities for solid-state NMR measurements to make contributions in the investigation of solid thin films because of the many problems facing nanotechnology and biotechnology that involve questions about the thin film state [2–4]. This paper provides a methodology and materials information that opens the door for performing solid-state proton NMR measurements on polymer thin films at non-cryogenic temperatures. Cryogenic approaches for performing thin film NMR experiments at mK temperatures were demonstrated [5].

To date, most studies [6] that use NMR to characterize organic materials with nanoscale dimensions have involved liquids, not solids, and have been directed towards infusing such materials into small confined spaces, such as are found in high surface area silica gels or vycor glasses. This approach maintains measurement sensitivity because the reduction in analyte density, relative to a bulk analyte, is typically less than a factor of five. These approaches, however, are not applicable for spin cast films on a flat substrate, especially for materials that vitrify upon cooling or loss of solvent where the thin film configuration and the processing steps are the primary variables of interest. One could fill gel pores with viscous melts at elevated temperature or fill with solutions from which the solvent will be removed in order to form the solid. Nevertheless, such approaches are subject to several concerns: material on the inside versus the outside of the porous media, the details of the preparation (e.g., complete versus partial pore filling), the nature of the equilibrated state within pore structures, and the existence

☆ Official contribution of the National Institute of Standards and Technology; not subject to copyright in the United States.

* Corresponding author. Address: Polymers Division, National Institute of Standards and Technology (NIST), 100 Bureau Drive, Gaithersburg, MD 20889-8541, USA. Fax: +1 301 975 3928.
E-mail address: vprabhu@nist.gov (V.M. Prabhu).
[1] Present address: Qualcomm, 2581 Junction Ave., San Jose, CA 95134, USA.
[2] Present address: Rhodia, 350 George Patterson Blvd., Bristol, PA 19007, USA.

1090-7807/$ - see front matter Published by Elsevier Inc.
doi:10.1016/j.jmr.2009.08.010

of concentration gradients that are likely to form as the analyte mixture penetrates the extensive pore network (e.g., chromatography-like separation of mixtures). In addition, the gel substrate is typically unoriented and does not lend itself to use of the substrate as an orienting surface. Finally, if one attempts to use proton spectroscopy, one must take account of extraneous signals that arise from the substantial number of gel-surface protons.

Two obvious reasons for the lack of NMR measurements of substrate-supported, flat, solvent-cast thin films include the potential for low sensitivity, when the film is very thin and the lack of availability of a sufficiently thin substrate that has minimal magnetic perturbation and contributes no interfering signal. The issue of sensitivity is most easily addressed by using proton (or ^{19}F detection if such nuclei are present), where we include experiments that use protons to detect other nuclei indirectly [7–10]. Yet the successful and robust use of proton detection in the solid must be accompanied by a substrate with no interfering signals.

There have been earlier attempts to address this class of problems using mica as a substrate in NMR experiments because it can be easily cleaved. For example, sandwiched layers of paramagnetic natural mica (15 × 15 mm, 30–60 μm thick) were used [11] to orient lipid bilayers and measure the in-plane diffusional motion. Thus, very broadband detection, typically used when dealing with rigid solids, was not necessary. Additionally, with mica planes placed perpendicular to the applied magnetic field and not spun, the paramagnetism of the mica mainly contributes to additional chemical shift when the sample thickness is much less than the distance across the mica planes [11]. In this case, the lipid layers were quite thick and it was feasible to detect ^{31}P rather than proton signals. In another reported [12] use of mica as a support for a true solid, a layer of oriented solid amyloid fibrils was deposited on the flat mica surface. Using magic-angle spinning with synchronized pulse sequences and ^{13}C detection, information about the orientation of chemical shift tensors relative to the fiber axis was obtained from the phasing of the spinning sidebands. Corrections for the paramagnetism of the natural mica were necessary to deduce this information; moreover, the layer thickness of the fibrils was chosen to be comparable to the substrate thickness in order to maintain sensitivity. Neither of the above uses of mica corresponds to a sub-micron thin film application.

One important motivation for studying thin films arises from the importance of measuring the degree of component mixing in thin film photoresist formulations. Such mixtures are used to pattern surfaces for integrated circuits. Major components of commercial photoresist formulations typically include a dominant matrix component (usually a polymer capable of a catalyzed solubility-altering reaction) and a minor, photo-activated, catalytic component called a photoacid generator (PAG). It is essential that the PAG be intimately mixed into the matrix especially as the lithographic dimensions approach macromolecular sizes. We conducted [13] proton NMR studies of mixing in several matrix/PAG systems using bulk, solution-cast mixtures to understand thermodynamic compatibility. However, the relevance of bulk studies to photoresist applications is not known because photoresist applications involve thin films with thickness less than 300 nm. In this case, specific thin film issues arise, such as the role of the solvent, especially with respect to the possibility of differential solubility of the photoresist components in the casting solvent and interface energetics that cause one component to have a higher concentration at a particular interface.

In order to extend the NMR techniques to the area of thin films, a relevant substrate is necessary. A silicon wafer with an oxidized surface as used by the microelectronics industry would be of practical interest. However, signal-to-noise considerations for NMR dictate that sub-micron thin films require a thin substrate. The layered structure of mica allows its splitting into thin sheets. Moreover, the structure of each mica layer (≈1 nm thick) consists of three sheet-like zones, i.e., a central octahedral sheet sandwiched between two tetrahedral sheets that form the surfaces. In common muscovite and phlogopite micas, the tetrahedral sheets are aluminosilicates with a 3:1 ratio of silicate to aluminate tetrahedra [14]. The preponderance of silicate in this surface leads to an expectation that surface energetics for mica and oxidized silicon are similar.

In this paper, we use both natural and synthetic mica as substrates for two-component, glassy, sub-micron thin films by solid-state proton NMR. These thin film systems consist of less than 2% by volume of analyte, when compared to a bulk sample. The synthetic mica has properties amenable for solid-state NMR owing mainly to its diamagnetism versus the strong paramagnetism that occurs with natural micas. Comparison of the results from the natural micas help demonstrate the real experimental advantages of the synthetic micas. In addition, we highlight the experimental strategies for moderating the paramagnetic influence of the natural micas. Therefore, the magnetic susceptibilities, both parallel and perpendicular to the mica plane, were independently measured to support the experimental findings and strategies.

We use proton spin diffusion [15] methods [16–19] to test mixing experimentally for two thin-film blend systems on synthetic mica. A well-defined proof of concept system consists of a 50/50 blend (by mass) of polystyrene (PS) and poly(xylylene ether) (PXE) that has been examined previously for mixing in the bulk by NMR [20]. The second system is a 95/5 (by mass) blend of poly(1-methyladamantyl methacrylate) (PMAdMA) and triphenylsulfonium perfluorobutanesulfonate (TPS-PFBS) which is a model photoresist system. This latter blend was challenging to characterize even in the bulk because of the disparate numbers of protons associated with each component.

The methods and materials introduced herein offer new possibilities for NMR characterization of solid thin films. For example, this opens the door for NMR studies of fundamental thin-film problems such as dynamic heterogeneity in glassy materials, phase transition and ordering phenomena of block copolymers, and self assembly of small molecules such as lipids and supramolecular structures.

2. Experimental

2.1. Materials

Two grades of naturally occurring muscovite mica were investigated: a visibly darker, commercial grade (S&J Trading, Inc., Glen Oaks, NY[3], grade: #1; quality: mixed, ruby V-1 and V2; thickness >0.18 mm and size >5 cm) and 2.5 cm diameter clear premium-grade disks (SPI Supplies, West Chester, PA; quality: V-1; thickness: 0.15 mm). The synthetic fluorophlogopite mica, $[KMg_3(AlSi_3O_{10})F_2]$, was manufactured by H.C. Materials, Inc. (Bolingbrook, IL; http://www.hcmat.com).

Polymeric materials used to make the thin films included a polystyrene (PS) NIST standard reference material (SRM 706, number-average relative molar mass, M_n, of 1.36×10^5 g/mol and mass-average relative molar mass, $M_w = 2.7 \times 10^6$ g/mol) that was cast from chloroform, an additive-free research sample of 50:50 (by mass) blend of PS and PXE obtained from General Electric (Schenectady, NY) also cast from chloroform, and PMAdMA [DuPont; $M_w = 9000$ g/mol] cast from cyclohexanone. TPS-PFBS was purchased from Sigma–Aldrich and used as received. Also,

[3] Certain equipment, instruments or materials are identified in this paper in order to adequately specify the experimental details. Such identification does not imply recommendation by the National Institute of Standards and Technology nor does it imply the materials are necessarily the best available for the purpose.

for the 95:5 (by mass) blends of PMAdMA with TPS-PFBS, solutions of each ingredient in cyclohexanone were first filtered and then combined in the proper proportions prior to spin coating. The chemical structures are provided in Scheme 1.

Thin films on the mica substrates were prepared in one of two ways. For the naturally occurring mica samples, a freshly cleaved surface was prepared. The mica was then placed onto a spin coater (Headway Research, Inc., Garland, TX), the solution was applied and spin cast. The sample was subsequently vacuum dried and mica further cleaved in air. For the synthetic mica samples, the mica was cleaved while submerged in distilled water as suggested by the manufacturer. We prepared two mica sheets with fresh surfaces and final thickness of (25 ± 10) μm. The mica required a mechanical support for spin coating. A droplet of reagent-grade toluene was placed on a clean silicon wafer that was, in turn, placed onto the spin coater. Then the mica layer was laid over the droplet, adhering to the substrate by capillary forces; then the solution was applied for spin coating. The non-solvent boundary, at the edge of the mica sheet, prevented wrap-around coating of the bottom of the mica sheet. Samples were then dried on a hot plate for 1 min at 130 °C. The polymer film thickness (either 250 nm or 500 nm, depending on the study) was determined using spectral reflectance (Filmetrics, Inc., San Diego, CA) and/or atomic force microscopy (Digital Instruments). After drying, the mica sheets could be separated from the substrate and, to assure a constant film thickness and to guard against any residual wrap-around coating, a thin perimeter from each mica sheet was cut away prior to preparing the NMR samples. Oriented stacked-disk samples were frequently used. These consisted of 4 mm outer diameter (OD) disks, stacked into the rotors such that the normals to the disk planes were parallel to the rotor axis. To make such disks, we cut the sample into strips of about 4.5 mm to 5 mm wide and proceeded to punch disks. We used a light hammer strike to a hole punch (with uniform 4 mm inner diameter (ID) and tapered OD) and employed a thick sheet of polytetrafluoroethylene as a working base. Initial cutting into strips prevents the undesirable propagation of cracks if one tries to punch disks from a wider mica sheet. For unoriented samples, the mica was cut with a sharp scissors into approximate squares that were between 1 mm and 1.5 mm on an edge.

2.2. Magnetic susceptibility

Magnetic susceptibility measurements were carried out using a MPMS® superconducting quantum interference device (SQUID) magnetometer (Quantum Design, San Diego, CA). Significant care was taken to prevent contamination of the mica samples, including, but not limited to, handling of the samples only with enamel coated tweezers to prevent contact transfer of ferromagnetic atoms [21]. After resetting the magnet to remove any trapped flux in the superconducting magnet (and therefore any field offsets), a hysteresis loop was measured at 298 K starting from +4 MA/m to −4 MA/m and back to +4 MA/m (+5 T/−5 T cycle of externally applied field), with the applied field either parallel or perpendicular to the mica surfaces. The susceptibility was obtained from the fitted slope of the curve, after normalization for sample mass and background corrections for the sample mountings.

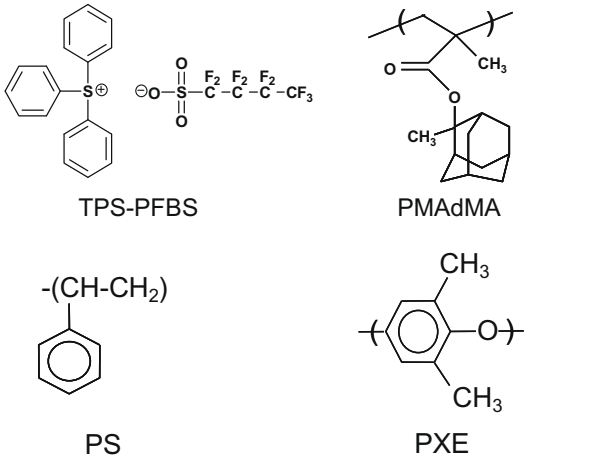

Scheme 1. Basic chemical structures, with acronyms, for the materials used in this paper. Triphenylsulfonium perfluorobutane sulfonate (TPS-PFBS), poly(1-methyladamantyl methacrylate) (PMAdMA), poly(styrene) (PS), and poly(xylylene ether) (PXE).

2.3. NMR methods

NMR measurements were carried out at ambient temperature on a Bruker Avance spectrometer (Bruker Biospin Corp., Billerica, MA) operating at 7.05 T (300 MHz for protons). Our low-background proton probe was manufactured by Doty Scientific (Columbia, SC) and has capabilities for handling high-power radio frequency (rf) and for magic-angle sample spinning (MAS). This probe uses 5 mm OD (4 mm ID) silicon nitride rotors and the active sample volume is restricted, using a pair of 2 mm thick poly(tetrafluoroethylene) spacers, to a 4 mm length in the middle of the rotor. Endcaps are made from poly(chlorotrifluoroethylene). Generally, rf amplitudes corresponded to proton nutation frequencies of 167 kHz (1.5 μs 90° pulses). Bloch-decay spectra were obtained using a dwell time of 1 μs and a 5 MHz filter width. The 1D pulse sequence, which we refer to as a chemical-shift-based spin diffusion (CSBSD) experiment, has been well described elsewhere [17,19] including the method of data analysis. Briefly, this sequence consists of 4 periods. In the *first period* one generates a chemical-shift-based initial polarization profile that is sinusoidally varying across the spectrum. This polarization gradient results from the application of a fixed number (10 or 20 in our case) of MREV8 [22,23] multiple-pulse cycles where each 8-pulse cycle time is 39.6 μs. MAS frequency was chosen to be 2525 Hz in order to minimize artifacts by satisfying the condition that there be an integral number (1 or 2) of rotor periods during the generation of this polarization (gradient) profile. The corresponding spectral period of the sinusoidal polarization variation is 8.4 ppm for the 20-cycle preparation and 16.8 ppm for the 10-cycle preparation. Following the conversion of the transverse magnetization into longitudinal magnetization (or polarization) at the end of the first period, the *second, variable period* of spin diffusion, t_{sd}, begins. No rf is applied during t_{sd}. In the *third period*, an MREV8 spectrum is obtained, from which the progress of spin diffusion as a function of the variable t_{sd} can be determined. Such spectra, which combine multiple-pulse and MAS techniques are called CRAMPS [24] spectra (combined rotation and multiple-pulse spectroscopy). During the *fourth period*, magnetization recovers to equilibrium.

Estimated uncertainties in measured quantities cited in this paper correspond to one standard deviation unless otherwise specified.

3. Results

3.1. Bulk magnetic susceptibility (BMS)

BMS values were measured for the three mica samples in both the parallel and perpendicular directions of B_o with respect to the plane of the mica. In addition, for the in-plane geometry, an arbitrary axis was chosen in the mica plane and three measurements were taken: the first with B_o parallel to that arbitrary axis and subsequent measurements differing by consecutive 45° rotations

about an axis normal to the plane. From these three measurements one can estimate (see Table 1 footnote) the in-plane susceptibility anisotropy as shown in Table 1. The two natural micas are quite paramagnetic, with the visibly darker, ruby mica having the strongest paramagnetism. Secondly, while the raw SQUID data are not shown, all data show a linear, hysteresis-free and reversible dependence on B_o indicating the lack of any significant contribution from magnetizable material or material that will saturate below 5 T at 298 K. This fact, however, does not preclude the possible existence in the natural micas of contaminating particulate sources of paramagnetism. At the same time, it is recognized [14] that in natural micas, paramagnetism is often associated with the presence of non-exchangeable Fe ions that substitute directly into the central octahedral sheets of each layer. Thirdly, the parallel/perpendicular anisotropy of the two natural micas is also such that the in-plane element is more paramagnetic (less diamagnetic) than is the perpendicular element; however, only the premium synthetic mica has an anisotropy that is a significant fraction of its mean value. The in-plane anisotropies for the synthetic and the ruby micas are significantly larger than the parallel/perpendicular anisotropies. In every case, however, the data show that those paramagnetic sources in the natural micas are more nearly isotropic than anisotropic since all the anisotropies are significantly less than the mean tensor values. Thus, in the presence of natural mica the CRAMPS technique, under MAS, will produce proton spectra whose increased spinning sideband intensities will be a more dominant issue than the corresponding loss of resolution. This follows since, for a film sample on mica, the spinning sideband (ssb) intensities relate to the maximum excursions in local field as the rotor turns; hence, ssb's should increase monotonically in intensity with the mean BMS (with a secondary dependence on the anisotropic part of the BMS tensor). In contrast, the loss of resolution can be traced to the *anisotropic character* of the BMS tensor; [25] hence, this effect will depend less directly on the mean susceptibility. From Table 1, the synthetic mica is expected to give weakest sidebands and best resolution.

In contrast to the paramagnetic natural micas, the synthetic mica is diamagnetic with a susceptibility almost an order of magnitude smaller than that of the natural micas. Moreover, the susceptibility anisotropy is correspondingly small, i.e., its isotropically averaged susceptibility, -3.70×10^{-9} m^3/kg, translates into a diamagnetic volume susceptibility in the range from (1 to 2) times that of most organic compounds [26]. Hence, we expect the resolution of the film that depends on the mica susceptibility anisotropy to be similar to bulk organic compounds. On the other hand, the ssb intensities are expected to be only modestly larger than the bulk. This follows since, for bulk rigid solids or those showing limited mobility, ssb intensities are largely determined by the respective chemical shift anisotropies (typically about 5 ppm [27]) of the various protons. For example, for a substrate with a susceptibility that is double the magnitude of the film layer, we expect a measureable increase in intensity for the ssb's.

A final note about Table 1 is that the generality of the results is only significant for the chemically well-defined synthetic mica; other measurements, while precise, cannot be generalized, owing to the natural origin of the material.

4. Solid-state proton NMR

4.1. CRAMPS spectra of bulk vs. thin-film samples using natural mica

Fig. 1 illustrates problems associated with the thin film CRAMPS spectra. Spectra 1A–1C relate to polystyrene (PS) and 1D–1F to the photoresist polymer, PMAdMA. These are one-sided Fourier transforms with the rf carrier frequency near the left side of the spectrum; hence aliasing issues (mirrored reflections of frequencies to the left of the carrier back to the right of the carrier) are particularly important in spectra with strong ssb's. Compared to the spectrum of bulk PS (1C), the unoriented thin-film sample (1A) showed a significant degradation in resolution as well as strong ssb's. Both an improvement in resolution and a reduction in ssb intensities were seen upon moving to the stacked disc geometry (1B). Similar, but even more dramatic gains were seen in the PMAdMA case for the stacked disc geometry (1F), relative to unoriented mica (1D). In fact, in 1F the resolution of the PMAdMA line looks comparable to that for the bulk (1E); only the ssb intensities in 1F are significantly higher than for the bulk. Two distinctive things about the film in 1F are: (a) the stacked discs occupy only about 40% of the normally used sample volume (empirically, thinner samples give some improvement in resolution), and (b) the film includes five mass percent of a photoacid generator (PAG). This PAG, TPS-PFBS, contains only aromatic protons (5–8 ppm range) at a level of about 1.5% of the total proton population. Note that the linewidth of the PMAdMA in 1F is now sufficient to identify the weak aromatic resonance of the PAG. Also, based on our observations for bulk samples, the PAG, that is well distributed in the PMAdMA lattice in bulk samples [28], has negligible impact on PMAdMA molecular mobility or CRAMPS linewidth; thus, PMAdMA linewidths in spectra 1D–1F can be compared, even though the samples are slightly different.

4.1.1. Synthetic mica

The available synthetic mica has two important characteristics. First, it is *diamagnetic*; hence, it should offer a significant reduction in linebroadening and ssb intensities. Second, it is fully fluorinated, i.e., there are *no interfering protons* associated with the mica, given that in naturally occurring mica, there is a particular site in the unit cell that typically has either a hydroxyl or a fluoride anion [14].

In Fig. 2, we show a comparison of CRAMPS spectra for three samples of a blend of 50/50 PS/PXE (by mass). Spectrum 2A is that of the bulk while 2B and 2C correspond to 250 nm thin film samples respectively as stacked-disks and unoriented. The latter sample was prepared as a collection of small rectangles that were

Table 1
Rationalized mass magnetic susceptibilites for micas in SI units of 10^{-9} m^3/kg.

Mica type	B_o|| 0°	B_o|| 45°	B_o|| 90°	Est. Mean B_o||[a]	$B_{o\perp}$	Δ(|| − ⊥)	In-plane (pk to pk)[b]
Synthetic	−3.73(5)	−3.85(10)	−3.06(8)	−3.39(20)	−4.11(4)	0.72(25)	1.14(40)
Natural premium	35.27(3)	34.38(2)	36.93(4)	36.10(9)	29.54(1)	6.56(10)	3.82(20)
Natural ruby	47.17(1)	49.13(1)	46.04(2)	46.61(4)	46.57(2)	0.04(6)	5.17(8)

Uncertainties (±) of one standard deviation, associated with the measurements themselves, aside from any contamination issues, are given in parentheses in units of the least significant figure.

[a] This estimated mean in-plane susceptibility is based on exactly fitting the three experimental in-plane measurements to an offset sinusoidal function, $Y = w + x \sin[2(\theta + z)]$, of fitted offset ($w$), phase ($z$) and amplitude ($x$). Y is the susceptibility in the table as a function of angle (θ) between B_o and a chosen direction in the mica plane where B_o is always in the plane of the mica.

[b] The values in this column are numerically equal to 2× as defined in note a, above.

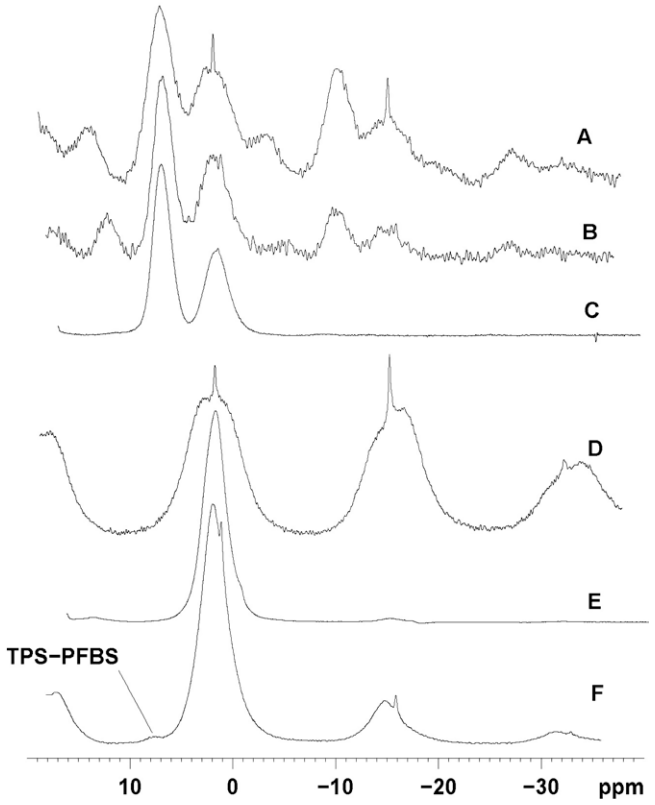

Fig. 1. CRAMPS spectra comparing bulk polymer samples (C and E) to 500 nm polymer thin films spuncast onto natural ruby (A, B, and D) and natural premium micas (F). PS thin film, unoriented (A), PS thin film, stacked-disc geometry (see text) (B), PS bulk (C), PMAdMA, thin film, unoriented (D), PMAdMA bulk (E), and 95/5 PMAdMA/TPS-PFBS thin film, stacked disc geometry (F). Note the increased linewidth and strong increase in spinning sideband intensity in the thin films, relative to the bulk samples and that the stacked disc geometry, relative to the unoriented samples, moderates these increases. The left side of each spectrum represents the carrier frequency; moreover, sideband intensities that should lie to the left of this point are reflected (aliased) back to the right. Chemical shift differences are accurate but shift positions are approximate (±0.5 ppm). Spectra of films on synthetic mica are nearly indistinguishable from bulk spectra (Fig. 2).

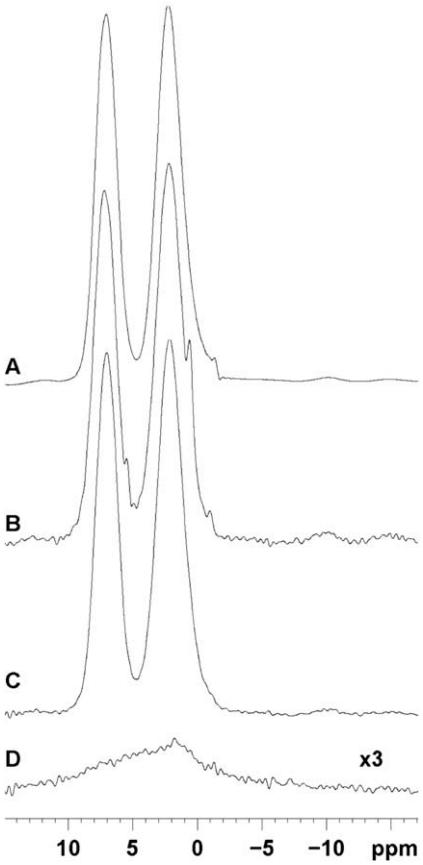

Fig. 2. Background-corrected CRAMPS spectra of 50/50 PS/PXE: unoriented 250-nm film on synthetic mica (A), stacked-disk 250-nm film on synthetic mica (B), bulk resin (C), and background spectrum (D) of the empty-probe that was subtracted, after proper scaling, from each signal (e.g., D is vertically amplified ×3 relative to A and represents about 11% of the total intensity).

poured into the rotor and pressed into the sample volume. Clearly, this sample is not randomly oriented and will tend to have some local ordering; however, there should also be a significant number of pieces at orientations far from having the mica normals along the rotor axis. The result is that the resolution of all three samples is indistinguishable. The ssb intensities of 2B and 2C are indistinguishable; moreover, the intensity of the first upper ssb (the one most intense and easily compared) at a MAS frequency of 2525 Hz is only about 50% higher in 2B and 2C relative to 2A. The ratio of aromatic and aliphatic first upper ssb's to the respective centerbands in 2B and 2C is (0.010 ± 0.001) and in 2A is (0.006 ± 0.001).

An important issue in Fig. 2 is relative sensitivity. The intensity ratio per scan in 2C relative to 2A is 1:57. In addition, all spectra have been necessarily corrected for contributions from the empty-probe (rotor plus sample-bracketing 2-mm-thick polytetrafluoroethylene plugs). The spectrum associated with background correction is shown in Fig. 2D, vertically amplified three times relative to Spectrum 2C. This background spectrum tends to show broad features over approximately a 20 ppm range; in the case of sample 2C, the integrated intensity of this correction represents 11% of the total signal. This is not a trivial correction, even for a probe designed to have a low-background intensity. We can, for example, test whether the background correction has been made reasonably well by looking at the ratio of aromatic to total intensity for the corrected spectrum and compare this with the theoretical value (0.451) for a 50/50 blend. Values for this ratio are (0.443 ± 0.003) in spectrum 2A and (0.438 ± 0.005) in spectrum 2C. These are close to theoretical and suggest that corrections are performed well; however, these integrals offer an indication that 2C has a slight excess of aliphatic intensity.

A final comment regarding Fig. 2 is that spectrum 2B also illustrates another aspect of sample purity. In 2B one can see small narrower resonances near 0 and 5 ppm which are not present in 2C. These additional impurities, associated with sample preparation of the stacked-disks, were largely avoided in preparation of the random rectangles. The level of interference of these additional impurities is observed in the spin diffusion spectra. The impurity near 5 ppm is probably water that has capillary condensed between the closely spaced mica layers that were frayed by the punching of the disks. The second impurity at about 0 ppm is probably a silicone-oil-type impurity most likely associated with the mold-release chemical from the latex gloves worn when punching the mica disks. These two impurities could be reduced by better handling and preparation techniques.

4.2. Spin diffusion spectra in a model blend: 50/50 PS/PXE

We began by measuring the degree of mixing in mixtures whose stoichiometry is closer to 50/50, rather than being dominated by one of the components (the latter situation typical of photoresist mixtures). Further, proton-NMR spin-diffusion techniques

[20] have been used to show that bulk samples of 50/50 PS/PXE are very well mixed.

Spin diffusion experiments were run for the three samples of Fig. 2. Figs. 3–5 give pertinent spectra, respectively, of the unoriented thin film, the stacked-disks thin film and the bulk resin. The spin diffusion spectra given in these figures have been adjusted to give zero-integral spectra by subtraction of appropriately scaled equilibrium spectra. Such subtraction preserves the polarization gradients, essential to the interpretation of the data, while allowing one to assay, visually and easily, via the disappearance (or lack thereof) of intensity, whether spin equilibrium has (or has not) been reestablished.

Spectra of the unoriented thin film in Fig. 3 represent our best opportunity to check on mixing for the thin film. All spectra are first corrected for background signals from the empty-probe by having run identical experiments and subtracted corresponding spectra. Spectrum 3A is that of the blend, 3B is that of a pure bulk PS sample, 3C is a difference spectrum, (3A–3B) representing an approximation to the PXE spectrum (we did not have a pure PXE sample). Spectrum 3C is scaled so that relative intensities for 3B and 3C correspond to that expected for a 50/50 blend. The ratio of aromatic to aliphatic intensities in 3C is also 1:3, consistent with the theoretical ratio and thereby verifying that the lineshape in 3C is a good approximation. Note that both the PS and PXE spectra have both aromatic and aliphatic intensities although they differ in intensity ratio. Hence, in the spin diffusion spectra, one cannot cleanly separate the PS from the PXE signals unless one is assured that the aromatic/aliphatic proton polarization gradients have vanished within each component. Spectra 3D–3Q are zero-integral spin diffusion spectra at the given spin diffusion times; vertical amplifications are also displayed. Spin diffusion, in the absence of relaxation, shows itself spectrally as a total-integral-preserving (adiabatic) process such that there is an apparent annihilation of equal amounts of positive and negative intensity. Most of the visible rapid intensity change is over for t_{sd} in the (2.5–4) ms range. Beyond these times, the intensity change is slow. Moreover, one does not get to a point where all intensity vanishes, a condition that would indicate sample-wide equilibration.

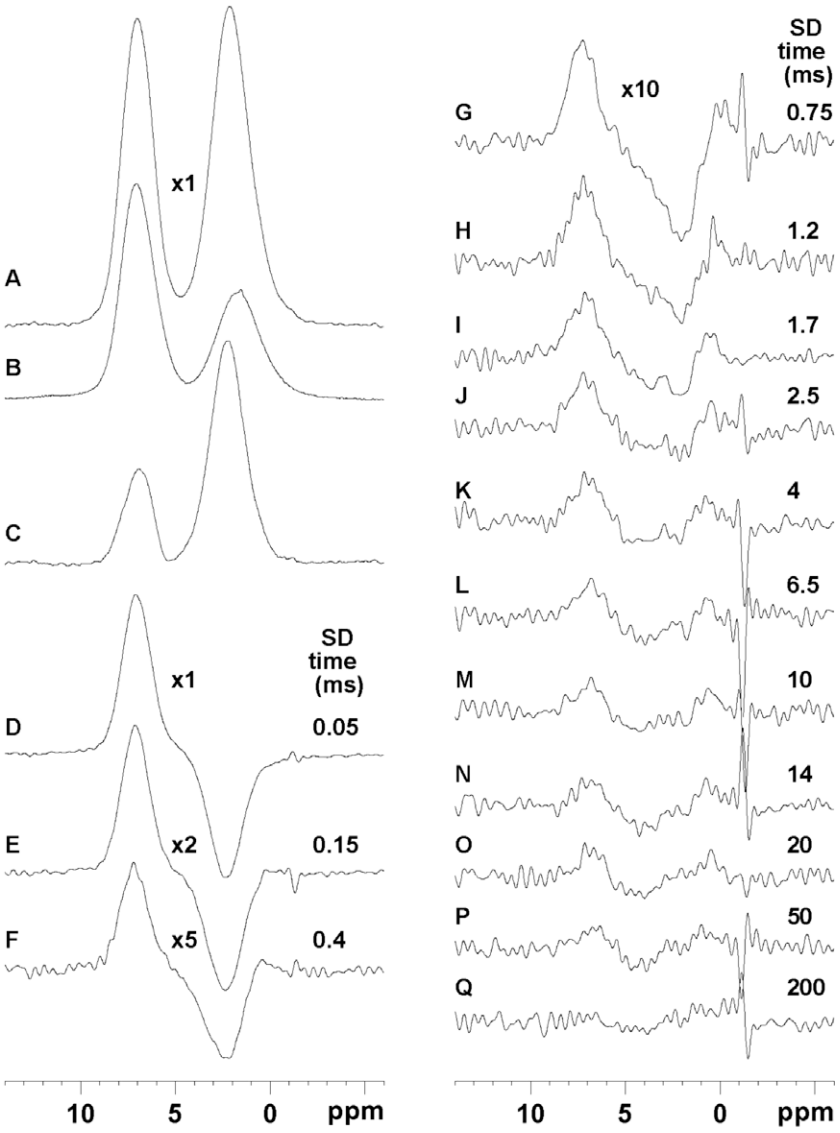

Fig. 3. Background-corrected CRAMPS spectra associated with the spin diffusion measurements on the 250-nm unoriented thin film of 50/50 PS/PXE on synthetic mica. Spectra are: equilibrium spectra of the blend (A), pure PS (B), and inferred spectrum of PXE (C = A − kB with k chosen to yield smooth line contours having the proper 3:1 aliphatic/aromatic intensity ratio). Spectra D–Q are zero-integral spin diffusion spectra associated with the indicated spin diffusion times and vertical amplification factors. An artifact at about −1.7 ppm appears at the spinning frequency relative to the rf carrier.

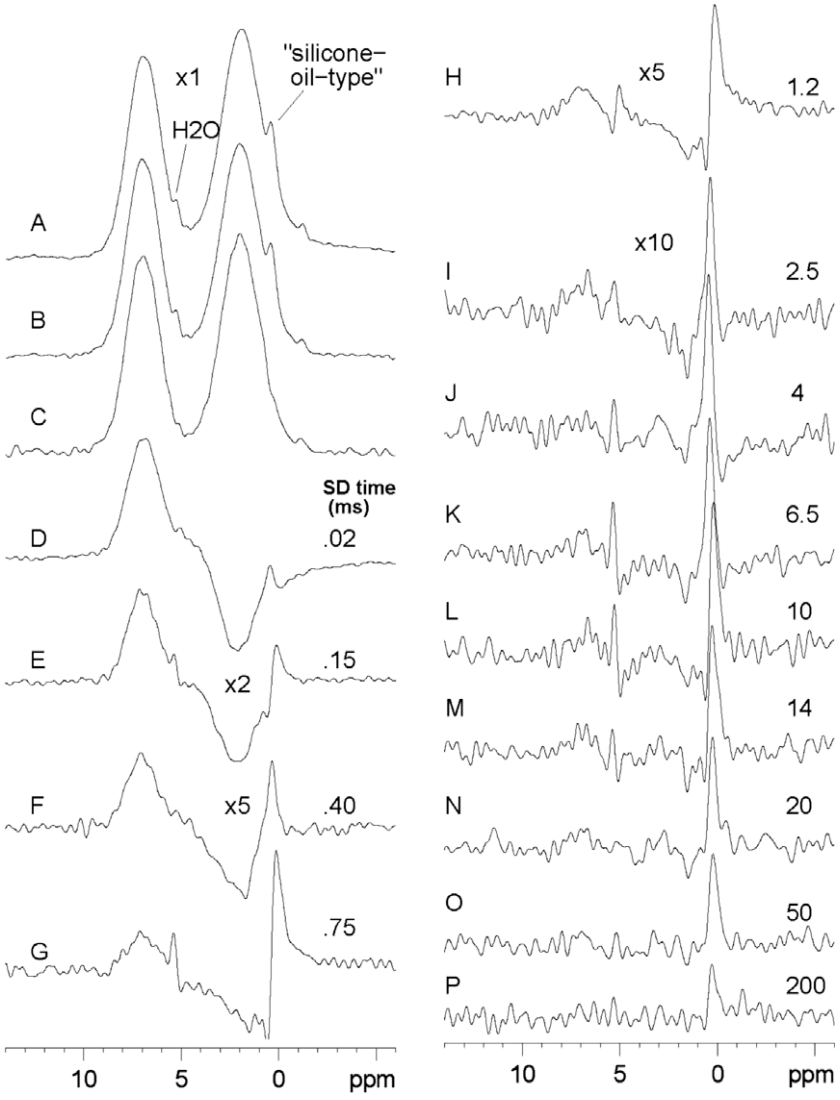

Fig. 4. Spectra similar to those in Fig. 3 corresponding to the stacked-disk sample of 250-nm thin film sample of 50/50 PS/PXE on synthetic mica. Other than the zero-integral spin diffusion spectra (D–P), A is the raw equilibrium spectrum, B has the empty-probe correction applied and C has an additional correction for the narrow water (≈5 ppm) and "silicone-oil" (≈0 ppm) resonances. We tried to make the "zero-integral" correction such that the contributions from the narrow impurity lines were ignored. Note, however, the phases of these narrower lines vary; hence, there is distortion of the adjoining blend resonances.

In this spin diffusion experiment, the initial polarization gradient is set up primarily between aliphatic and aromatic protons. Hence, the early time behavior is dominated by the process of spin equilibration within the two homopolymers. This is the fastest process. If the two polymers are intimately mixed, then, on a comparable, but slightly longer timescale, one will see heteropolymer spin equilibration, i.e., that equilibration process we are most interested in. As a first approximation in the spin diffusion analysis, we isolate the individual signals by (a) measuring the initial aromatic/aliphatic polarizations, (b) mapping the latter into a unique *initial average-polarization* gradient between PS and PXE protons (this would be the outcome if homopolymer equilibration happened instantaneously without any heteropolymer spin diffusion), and (c) interpreting observed aromatic/aliphatic ratios, as a function of spin diffusion time, t_{sd}, under the assumption that homopolymer spin diffusion is complete. This analysis procedure has been explained in the literature [29], however, the simplifying notion is that, by assuming instantaneous homopolymer equilibration, one can establish a normalized parameter, $\Delta M_s(t_{sd})$, that approximately monitors the heteropolymer spin equilibration, recognizing that at the earliest times, when homopolymer equilibration is still happening, the extent of heteropolymer equilibration will thereby be underestimated. However, at longer values of t_{sd}, $\Delta M_s(t_{sd})$ will be an accurate and appropriately scaled quantity. Assuming that homopolymer equilibration is complete, scaling is such that if heteropolymer equilibration has not yet begun, $\Delta M_s(t_{sd}) = 1.0$, and if heteropolymer equilibration is complete, $\Delta M_s(t_{sd}) = 0$. Thus, at the earliest times, the approximation to $\Delta M_s(t_{sd})$ typically well exceeds 1.0 and then proceeds to fall quickly to or below 1.0 as homopolymer spin equilibration goes to completion. In the case of this blend, $\Delta M_s(t_{sd})$ is quite reliably reporting heteropolymer spin diffusion for $t_{sd} > 1$ ms [20].

Figures showing spin diffusion spectra for the stacked-disk thin film (Fig. 4) and for the bulk blend (Fig. 5) are similar in format to Fig. 3, except that component spectra are not shown. Three things are of note in Figs. 4 and 5. First, in Fig. 4, the weak but narrow resonances of both the water and the silicon-oil-type impurities are evident and of somewhat varied phase. These intensities, with their corresponding phase distortions, make the determination of the broader polymer intensities more uncertain. Second, for the

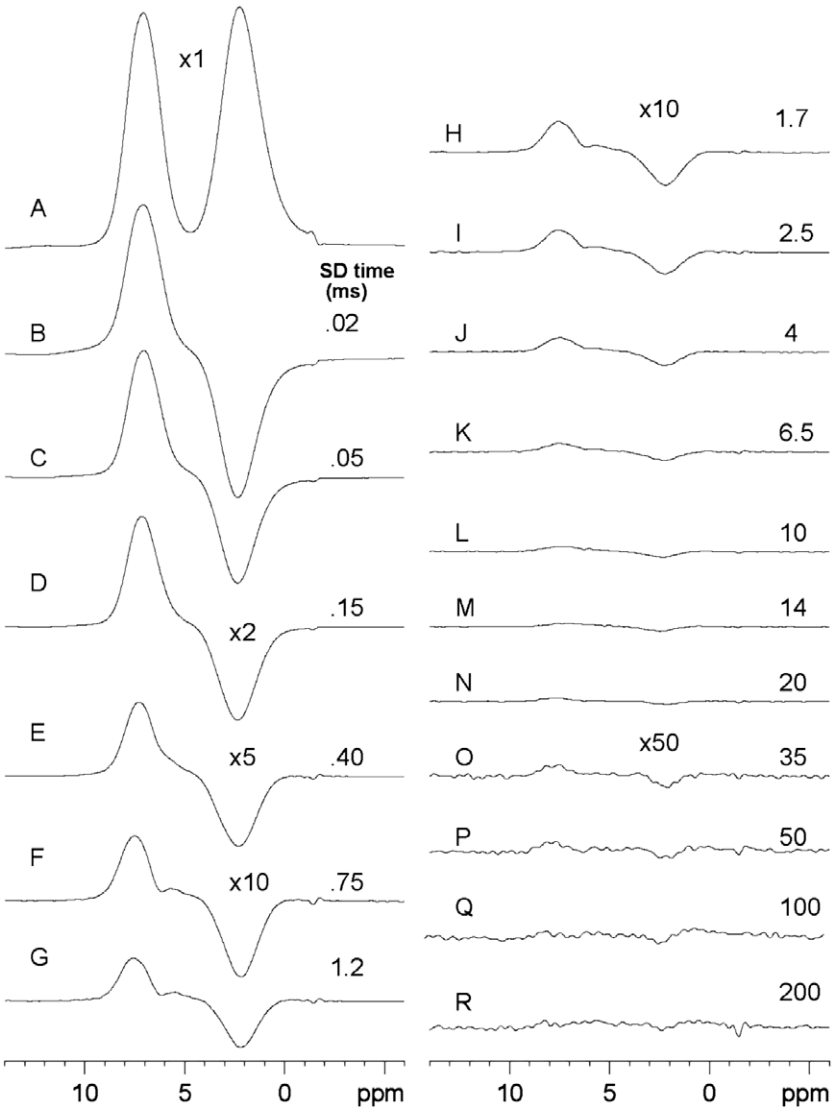

Fig. 5. Spectra of bulk samples of 50/50 PS/PXE for comparison with spectra of the synthetic unoriented mica disks (Fig. 3) and of the oriented stacked-disks (Fig. 4). Using the '×10' vertical amplification in the column on the right allows direct comparison with similar spectra in Figs. 3 and 4 showing that spin equilibrium returns more completely in the bulk sample.

bulk sample in Fig. 5, it is readily apparent from spectral comparison that the bulk spin system comes much closer to sample-wide equilibrium at longer times than do the thin film samples of Figs. 3 and 4. Third, as expected, signal-to-noise is overwhelmingly better for the bulk sample with each spectrum representing about 1000 scans for the thin film samples and about 200 scans for the bulk sample.

Fig. 6 shows a typical spin diffusion plot of $\Delta M(t_{sd})$ vs. $(t_{sd})^{1/2}$ and includes data for the bulk and the unoriented thin film; the bulk data are superposable on previously published bulk data for this blend [20]. The thin-film data fall rapidly at early times, mimicking the bulk behavior, but data deviate from the bulk at longer times. Qualitatively, the thin-film data imply the intimacy of mixing of the PS and PXE are comparable to the bulk, thus accounting for the rapid initial fall in $\Delta M_s(t_{sd})$. However, the curve approaches zero very slowly and stays about (0.05 ± 0.01) above the bulk data for $t_{sd} > 3$ ms which implies that the 50/50 stoichiometry varies over distances substantially exceeding 50 nm. Extreme examples of stoichiometric variations that would give account for a 0.05 asymptote for $\Delta M_s(t_{sd})$ involve a separation of either 9.5% of the

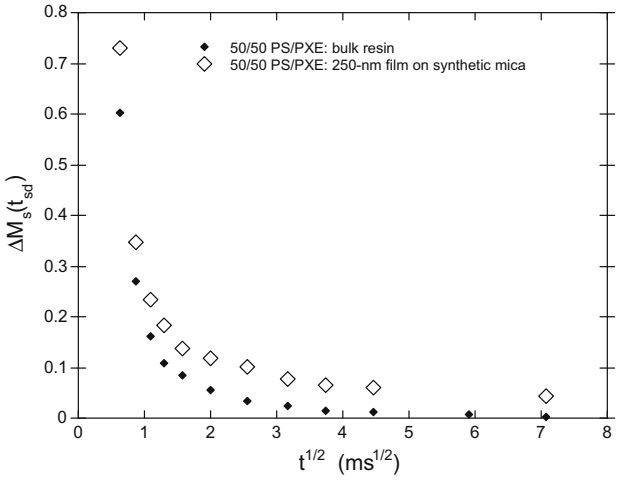

Fig. 6. Spin diffusion plot generated from spectra of Figs. 3 and 5. Uncertainty in each data point is indicated by the size of the symbol.

PS or 10.9% of the PXE into a pure, very large domain with the respective remainder uniformly and intimately mixed. Other stoichiometric variations could also be invoked to explain the same asymptote; these explanations would involve larger fractions of the materials and only mixed phases. The major question is whether this indication of compositional inhomogeneity is a real effect or whether this disparity between bulk and thin film behavior could have another explanation, e.g., some impurity. We revisit this question in the Discussion section. In any case, there is strong evidence of extensive intimate mixing from these thin film results.

4.3. Spin diffusion spectra in a model photoresist blend: 95/5 PMAdMA/TPS-PFBS

Owing to the strong disparity in stoichiometry between the components, the characterization of this mixture is challenging since the theoretical fraction of protons associated with the TPS-PFBS at 5% by mass is only 1.5%. The simplifying aspect of this mixture is that the TPS-PFBS protons are entirely aromatic and, in the presence of the synthetic mica, are expected to be spectrally distinct from the entirely aliphatic proton signals of the polymeric PMAdMA. The real question about applying this technique is whether there is adequate sensitivity for information about the mixing of the components. Based on the foregoing blend results, we expect difficulty in achieving adequate sensitivity. Yet, from the limited data, it is possible to make a qualitative comment about mixing owing to the spectral separation of aromatic and aliphatic component signals. The aromatic signal at shorter times can be followed to capture the initial, stronger change in PAG polarization. Such data qualitatively point to the intimate distribution of PAG in the PMAdMA even though corresponding information about the *uniformity* of mixing is not available.

We took data on both the stacked-disks and the scissor-cut, unoriented rectangles. As with the PS/PXE experience for the stacked-disk sample, we found a notable contamination by the silicone-type resonance (near 0 ppm) and condensed water (near 4.7 ppm). These resonances interfered with the interpretation of the spin diffusion spectra similarly to that shown in Fig. 4. Thus, we will only discuss spectra obtained from the unoriented sample. Resolution and spinning sideband intensities for the two preparations are comparable; hence, there is no disadvantage in using the unoriented sample.

Fig. 7 shows scaled equilibrium spectra for the unoriented 250 nm thin film (7A) and the bulk samples (7B) along with several spin diffusion spectra (7C–7M). Spectra have all been corrected for background signals from the empty-probe using data collected in

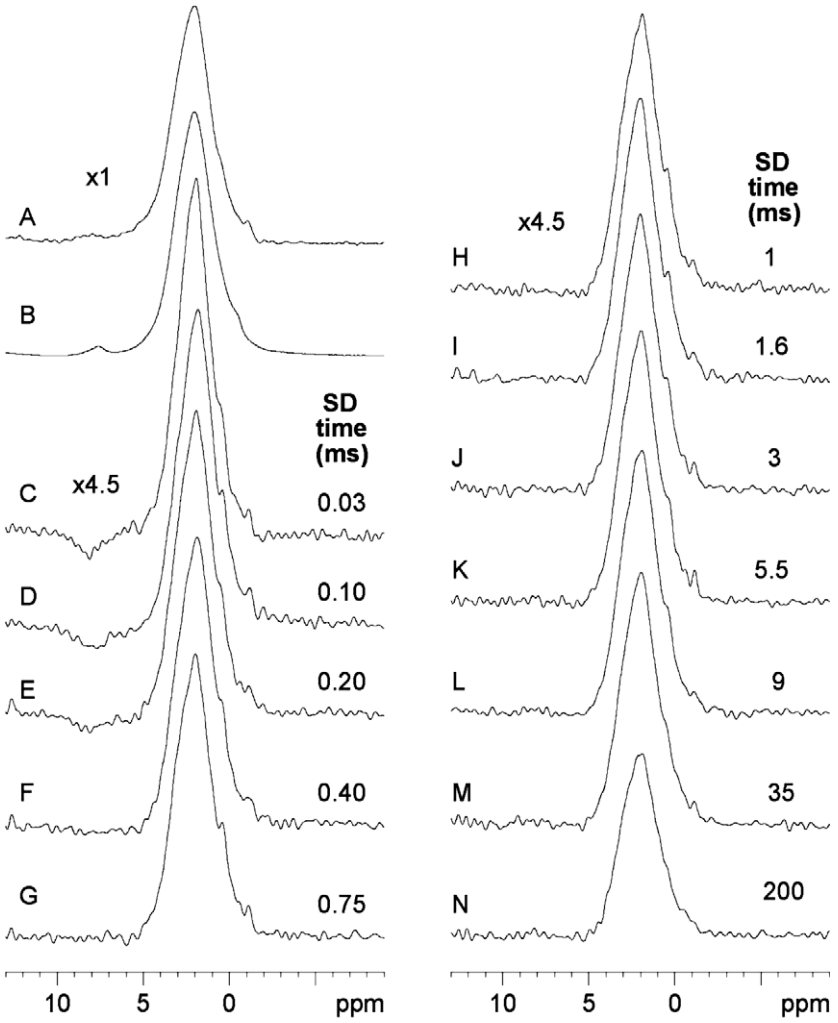

Fig. 7. Spin diffusion spectra, except B, associated with the photoresist blend, 95/5 PMAdMA/TPS-PFBS on synthetic mica. PMAdMA signals entirely reside in the big aliphatic peak while the TPS-PFBS signals (theoretically 1.5% of the total intensity) are entirely at 7 ppm. Equilibrium CRAMPS spectra: 250-nm thin film on synthetic mica (A), bulk sample (B). Spectra C–N are background-corrected spin diffusion spectra; however they are NOT zero-integral spectra, being about 21% of the equilibrium intensity. The spin diffusion spectra illustrate three things: (a) In C and D, the initial polarization gradient is quite strong and (b) after about 1 ms of spin diffusion, the aromatic wing is no longer negative and, (c) at longer times, the signal-to-noise ratio is hardy adequate to determine whether spin equilibrium has returned as judged by confirmation of a slight positive intensity in the aromatic region.

duplicate but separate experiments. However, in distinction from Figs. 3–5, the spin diffusion spectra in Fig. 7 are not presented as "zero-integral" spectra, but with the original intensities that were on average 21% of the equilibrium intensity.

In both spectra 1A and 1B the weak resonance in the (5–9) ppm range corresponds to the aromatic PAG resonance while the dominant aliphatic resonance is that of the PMAdMA. Note in 1A that there is no distinct peak near 0 ppm or 5 ppm, associated with silicone or water impurity protons. The shape of the aromatic resonance near 7 ppm in spectrum 7B is somewhat sharper than that in 7A since it was found that when chloroform or tetrahydrofuran were used as the casting solvents for the bulk samples, a liquid-like fraction of the PAG remained phase separated. Hence, the aromatic signal in 7B arises from a combination of liquid-like and solid environments for the PAG molecules and that explains the sharper attributes in 7B relative to 7A. Correspondingly, the absence of a sharper peak in 7A is taken as evidence that phase separation did not occur when the casting solvent was tetrahydrofuran.

In Fig. 7, at short t_{sd}, one can identify negative intensity in the aromatic region associated with a strong initial polarization gradient between aromatic PAG and aliphatic PMAdMA protons. Within the signal-to-noise, the negative PAG intensity is no longer obvious after 0.5 ms. For $t_{sd} \geqslant 9$ ms there is a hint of positive intensity in the aromatic region but, owing to the limited signal-to-noise, one cannot be sure, given that the aromatic intensity in the equilibrium spectrum (1A) is very small. Hence, based on the early time behavior alone, there is a rapid change in aromatic polarization, as expected from intimately mixed phases. However, we cannot be quantitative about the extent or uniformity of mixing.

5. Discussion

It is clear that synthetic mica represents an opportunity for characterizing thin films, including the investigation of the intimacy of mixing in blends. The critical issues are sensitivity and dealing quantitatively with extraneous signals associated with the probe, rotor, and spacers and those that appear by contamination during handling.

Higher magnetic fields and/or extensive signal averaging can partially address the sensitivity problem. In principle, sufficient signal averaging can always overcome signal-to-noise problems; however, for us there are also practical problems associated with extensive signal averaging. First, CRAMPS spectra are sensitive to spectrometer instabilities in rf amplitude and phase, i.e., slow drifts in rf amplitude and phase can have an impact on the reproducibility of spectra. We address these issues, in part, using block averaging (frequently repeating passes through the entire range of experiments as scans are accumulated), with the result that each spectrum in a set is subject to similar instabilities. The second issue is that the high rf duty cycle associated with the CRAMPS method causes accelerated aging of the receiver circuitry; hence, we were reluctant to expend a significant fraction of the receiver's lifetime on one sample by calling for 10 s of thousands of accumulations per spectrum. Most importantly, there is the question whether one is limited mainly by sensitivity or by other factors, e.g., corrections for spurious signals as we will discuss in the following paragraphs. Clearly, if one cannot deal with the latter corrections with high accuracy, then moving the signal-to-noise ratio beyond a certain limit is not practical because the interpretation is no longer limited by signal-to-noise. This was the case for the PS/PXE thin films we investigated. In that case, we found that (1000–2000) scans produced sufficient signal-to-noise so that we were no longer limited in our interpretation by signal-to-noise.

The extraneous signals from the probe, rotor, and spacers can, in principle, be compensated for, although it takes extensive experimental time to produce these spectra since one would like to duplicate, using the empty rotor, each spectrum taken. In fact, one would like more scans associated with the empty-probe experiments in order to retain as much signal-to-noise in the corrected sample spectra. However, the measured background signals with the CRAMPS technique cannot exactly reproduce the tuning in any two MP experiments. Slight shifts in the tuning leads to small changes in both phase and the apparent chemical shift offset. Hence there can be small changes in phase and effective chemical shifts (typically less than 0.5 ppm) between acquisition of sample and background spectra. Since the background signals have some typical dependence on offset from the carrier frequency, the subtractions will thus not always be exact.

Extraneous signals that arise from sample contamination can be minimized through careful sample preparation. Such contamination can be introduced in various ways including: handling during initial cleaving of the mica sheets, impurities in solvents and solutes, contamination from the atmosphere, handling of thin-film materials in preparation for placement in the rotor, and layer fraying in the cutting of the mica materials that eventually induces water condensation.

The spin diffusion data for the both the stacked-disk and unoriented thin films of PS/PXE showed incomplete equilibration and the question arises whether this represents some true heterogeneity in the thin films that is not present in the bulk samples or whether a small amount of aliphatic contaminant could give rise to this result. Considering the initial polarization levels for the aliphatic protons and the amplitude differences between the aliphatic and aromatic signals in Figs. 3 and 5 for $t_{sd} > 6$ ms, one can calculate that it would take an aliphatic contamination level of about (1.0 ± 0.2)% of the total proton intensity to produce this result, so long as that contaminant did not undergo spin diffusion with the polymers. Recall, that, after corrections for background intensity, the ratios of aromatic to total intensity measured for this sample and the bulk sample were (0.438 ± 0.002) and (0.443 ± 0.001), respectively, compared to a theoretical value of 0.451 for a 50/50 blend. If we presume that the disparity between 0.443 and 0.451 in the bulk sample arises from a systematic error in integration, then the thin-film ratio ought to be 0.005 less than the bulk ratio (as is observed) if there is aliphatic contamination in the thin-film at a level of 1% of the total protons. While this is not conclusive proof that such a contamination exists, it is plausible based upon the self-consistency of the estimated contamination level from the spin diffusion data and from the relative intensity of the aromatic line. But, aside from these arguments, we really cannot determine, based on the NMR evidence alone whether or not the PS/PXE is mixed well, such that there are no large-scale inhomogeneities in concentration. Differential solubility of the two-components in the casting solvent presents the most likely explanation if the thin-film spin diffusion data is truly pointing to compositional inhomogeneity. To our knowledge there are no independent thin-film studies that indicate any tendency for this blend to demix.

Natural mica leads to high background signals and paramagnetism that causes unacceptably intense spinning sidebands and linebroadening. While this may be reduced using a stacked-disk geometry, their levels remain a limiting problem. In contrast, the synthetic mica is advantageous as a substrate for thin films, both from the points of view of susceptibility, susceptibility anisotropy and the lack of interfering proton background signals arising from the mica lattice. One also need not use oriented samples with synthetic mica. This latter simplification makes sample preparation much easier and, for us, allowed us to work with mica pieces that avoided the layer fraying associated with our attempts to cut disks. Layer fraying led to water condensation and detectable, interfering water signals.

Finally, an experimental parameter that has an impact on sensitivity is the film thickness and the thickness of the mica sheets. We

chose to increase the signal-to-noise by working with 250 nm thick polymer films. Depending on the questions one wishes to address, going to thinner films will make it harder to contend with extraneous resonances, even though there is adequate sensitivity for simply detecting signals from films even in the 50 nm range. As to the matter of mica sheet thickness, we managed to cleave sheets to a nominal thicknesses in the range of (25 ± 10) μm with edge dimensions of (3–5) cm. Obviously, one would get a significant potential increase in sensitivity by using thinner mica sheets.

There is one issue regarding natural mica that is worth noting. The hydroxyl protons in the natural mica lattice, whose spectral broadening is dominated by electron–proton dipolar interactions associated with Fe impurity sites, are also quite isolated magnetically from other protons. Since multiple-pulse techniques are designed to eliminate proton–proton dipolar interactions while only modestly scaling interactions linear in the proton magnetic moment, such techniques do an incomplete job of narrowing these mica-related resonances. As a result, these proton background signals from inside the mica layers are much more visible in the Bloch-decay spectra versus in the CRAMPS spectra. In both kinds of spectra, these resonances are broad; however, in the CRAMPS spectra, with their narrower spectral range, the mica-lattice protons tend to look like contributions to the baseline where they can largely be ignored. Thus, based on contrasting linewidths, separation of mica-lattice proton signals from the thin-film signals in paramagnetic natural mica is more easily accomplished in CRAMPS spectra compared with Bloch-decay spectra.

6. Conclusions

It is shown that solid-state proton spectra, especially CRAMPS spectra, of organic thin-films on synthetic fluorophlogopite mica show comparable levels of resolution and spinning sideband intensities compared with bulk samples, even when samples consist of unoriented, volume-dominating mica pieces. In contrast, similar thin-film samples utilizing natural paramagnetic muscovite micas show degraded resolution, large spinning sidebands and interfering proton signals. The feasibility of studying mixing in polymeric thin-film blends has also been demonstrated as an application using synthetic mica as a thin-film substrate. The samples we looked at were about 250 nm thick and NMR signals, by integration, were typically down about a factor of 50–75 in sensitivity, relative to bulk powder samples. This reduced sensitivity will have contributions from differences in packing efficiencies for powders versus mica flakes as well as averaging over small variations in polymer film thickness and mica thickness. We generally produced a range of acceptable mica thicknesses in the range of (25 ± 10) microns and then tended to select the thinner sheets if available. We do not imply that 25 μm is an average value.

The high sensitivity of proton NMR in combination with attention to clean sample preparation and handling should allow investigations of thin films down to a few tens of nm, where, ultimately, through signal averaging, the limit of the technique will depend, not on the mica characteristics, but on reducing extraneous background and impurity signals. The spin diffusion studies that we focused on are especially sensitive to impurities, whereas other NMR experiments will be much less sensitive. Not all experiments one might wish to do on thin films use multiple-pulse techniques, which, in our case, made it harder to make precise corrections for signals arising from the empty-probe. However, if multiple-pulse techniques are used, a productive improvement would be to find a way to tune a probe reproducibly and precisely from one sample to the next.

Fast-MAS techniques, involving rotational frequencies in the range of 30–70 kHz, also achieve a significant amount of chemical shift resolution for proton spectra. In some instances, fast-MAS techniques might replace multiple-pulse techniques in the characterization of thin films. However, the effectiveness of Fast-MAS for achieving resolution favors higher spinning speeds, high magnetic fields and protons with weaker proton–proton dipolar couplings [30]. For thin-film applications which examine component mixing, as has been illustrated in this paper, fast-MAS is not suitable for three reasons: first, fast-MAS slows down spin diffusion making the interpretation of mixing difficult. Secondly, at modest magnetic fields, such as was used in this paper, resolution under fast-MAS will remain inferior to that achievable with multiple pulse. Thirdly, there is a sensitivity issue in that the filling factors associated with sample volumes for fast-MAS are significantly smaller and this will entail some further loss of sensitivity; however, sensitivity improvement via extensive signal averaging is more practical using fast-MAS.

Finally, there are possibilities [7–10] for observing less susceptible nuclei with enhanced sensitivity via proton observation and indirect detection. Often those methods will incorporate pulse sequences that have the advantage of naturally rejecting impurity contributions.

Acknowledgment

We are indebted to Dr. Patricia McGuiggan who alerted us to the existence of the synthetic mica.

References

[1] K. Schmidt-Rohr, H.W. Spiess, Multidimensional Solid-State NMR and Polymers, Academic Press, London, 1994.
[2] The National Nanotechnology Initiative, National Science and Technology Council, Committee on Technology, 2008, http://www.nano.gov/NNI_Strategic_Plan_2007.pdf.
[3] C.T. Black, R. Ruiz, G. Breyta, J.Y. Cheng, M.E. Colburn, K.W. Guarini, H.C. Kim, Y.I.B.M. Zhang, J. Res. Dev. 51 (2007) 605–633.
[4] A.N. Shipway, E. Katz, I. Willner, Chemphyschem 1 (2000) 18–52.
[5] R.W. Singerman, R.C. Richardson, J. Magn. Reson. A123 (1996) 168–173.
[6] G. Buntkowsky, H. Breitzke, A. Adamczyk, F. Roelofs, T. Emmler, E. Gedat, B. Grünberg, Y. Xu, H.-.H. Limbach, I. Shenderovich, A. Vyalikh, G. Findenegg, Phys. Chem. Chem. 9 (2007) 4843–4853.
[7] Y. Ishii, R. Tycko, J. Magn. Reson. 142 (2000) 463–469.
[8] M. Hong, S. Yamaguchi, J. Magn. Reson. 150 (2001) 43–48.
[9] B. Reif, R.G. Griffin, J. Magn. Reson. 160 (2003) 78–83.
[10] E.K. Paulson, C.R. Morcombe, V. Gaponenko, B. Dancheck, R.A. Byrd, K.W. Zilm, J. Am. Chem. Soc. 125 (2003) 15831–15836.
[11] J.K. Rainey, B.D. Sykes, Biophys. J. 89 (2005) 2792–2805.
[12] N.A. Oyler, R. Tycko, J. Am. Chem. Soc. 126 (2004) 4478–4479.
[13] D.L. VanderHart, V.M. Prabhu, E.K. Lin, Chem. Mater. 16 (2004) 3074–3084.
[14] M.F. Brigatti, S. Guggenheim, in: P.H. Ribbe (Ed.), Reviews in Minerology & Geochemistry, Minerological Society of America, Washington, DC, 2002, p. 46. Chapter 1.
[15] A. Abragam, The Principles of Nuclear Magnetism, Oxford University Press, London, 1961. Chapter V.
[16] M. Goldman, L. Shen, Phys. Rev. 144 (1966) 321.
[17] P. Caravatti, P. Neuenschwander, R.R. Ernst, Macromolecules 18 (1985) 119.
[18] Ref. 1, Chap. 13.
[19] G.C. Campbell, D.L. VanderHart, J. Magn. Reson. 96 (1992) 69.
[20] D.L. VanderHart, Macromolecules 27 (1994) 2837–2845.
[21] D.W. Abraham, M.M. Frank, S. Guha, Appl. Phys. Lett. 87 (2005) 252502.
[22] W.-.K. Rhim, D.D. Elleman, R.W. Vaughan, J. Chem. Phys. 59 (1973) 3740.
[23] P. Mansfield, J. Orchard, D.C. Stalker, K.H.B. Richards, Phys. Rev. B7 (1973) 90.
[24] L.M. Ryan, R.E. Taylor, A.J. Paff, B.C. Gerstein, J. Chem. Phys. 72 (1980) 508.
[25] D.L. VanderHart, W.L. Earl, A.N. Garroway, J. Magn. Reson. 44 (1981) 361.
[26] R.C. Weast (Ed.), Handbook of Chemistry and Physics, The Chemical Rubber Co., Cleveland, 1971, p. E-119ff.
[27] M. Mehring, Principles of High Resolution NMR in Solids, Springer-Verlag, Berlin, 1983. pp. 238–239.
[28] Unpublished results from our laboratory.
[29] D.L. VanderHart, G.B. McFadden, Solid State Nucl. Magn. Reson. 7 (1996) 45–66.
[30] A. Samoson, T. Tuherm, Z. Gan, Solid State Nucl. Magn. Reson. 20 (2001) 130–136.